Vibration Analysis of Angle-Ply Laminated Composite Plates with an Embedded Piezoceramic Layer

Hsien-Yang Lin, Jin-Hung Huang, and Chien-Ching Ma

Abstract—**An optical full-field technique, called amplitude-fluctuation electronic speckle pattern interferometry (AF-ESPI), is used in this study to investigate the force-induced transverse vibration of an angle-ply laminated composite embedded with a piezoceramic layer (piezolaminated plates). The piezolaminated plates are excited by applying time-harmonic voltages to the embedded piezoceramic layer. Because clear fringe patterns will appear only at resonant frequencies, both the resonant frequencies and mode shapes of the vibrating piezolaminated plates with five different fiber orientation angles are obtained by the proposed AF-ESPI method. A laser Doppler vibrometer (LDV) system that has the advantage of high resolution and broad dynamic range also is applied to measure the frequency response of piezolaminated plates. In addition to the two proposed optical techniques, numerical computations based on a commercial finite element package are presented for comparison with the experimental results. Three different numerical formulations are used to evaluate the vibration characteristics of piezolaminated plates. Good agreements of the measured data by the optical method and the numerical results predicted by the finite element method (FEM) demonstrate that the proposed methodology in this study is a powerful tool for the vibration analysis of piezolaminated plates.**

I. Introduction

Over the past several years, the rapid development of piezoelectric materials has stimulated extensive research into important applications such as the electromechanical transducers, underwater acoustics, resonators, ultrasonics, and micro electromechanical systems (MEMS). Most of these engineering applications are successfully achieved by using the piezoelectric effect. Generally, the piezoelectric effect is classified into two types: the direct effect is typically used to generate a low impedance voltage signal from an input external loading, and the inverse effect is used to generate the induced mechanical deformation that corresponds to the applied electrical field. However, with the increasing demand and ongoing efforts for advancing performance of the conventional piezoelectric materials, it has become evident that the most common form of the piezoelectric materials, such as lead zirconate titanate (PZT) and polyvinylidene difluoride (PVDF), cannot fully satisfy the practical demands in engineering. To obtain the piezoelectric material with enhanced capabilities and to achieve the desired electromechanical and structural properties, many piezoelectric materials are incorporated into piezolaminated composites with fiber-reinforced layers. By combining different materials, the advantages of each ply can be exploited and the achieved performance is generally unattainable by the individual constituents. Hence, the study of the static and dynamic responses in piezolaminated composites has received considerable attention in recent years. Ha *et al.* [1] used an eight-node composite brick element and variational principle to construct the FEM formulation for modeling the dynamic and static response of laminated composites containing distributed piezoceramics subjected to both mechanical and electrical loadings. Abramovich and Livshits [2] used the principle of virtual work to study the dynamic behavior of cross-ply, nonsymmetrical composite beam with a uniform piezoelectric layer. Batra and Liang [3] used the three-dimensional linear theory of elasticity to study the vibrations of simply-supported rectangular laminated plate with embedded PZT layers; numerical results for a thin and a thick plate with one embedded actuator layer and one embedded sensor were presented. Bhattacharya *et al.* [4] developed a finite element formulation that considered the linear piezoelectric constitutive relations and the first shear deformation behavior to study the effects of stacking sequences, geometric boundaries, and the applications of electrical voltages on the vibration frequencies of laminated composite beams and plates that were surface bonded or embedded a set of piezoelectric layers. Loja *et al.* [5] presented a family of B-spline, higher-order finite strip models for the static and free vibration analysis of laminated plates with embedded or surface bonded piezoelectric laminate or patches. The advantage of such a piezolaminated structure is that the sensing and actuating mechanisms become part of the structure. It is especially apparent for the lightweight composites used as the major structure and might be deployed in space. Hence, the development of piezolaminated composite materials offers great potential for uses in advanced aerospace structural

Manuscript received November 28, 2002; accepted April 4, 2003. The authors gratefully acknowledge the financial support of this research by the National Science Council, Republic of China, under Grant NSC 90-2212-E-002-163 (C.C.M.) and 91-2212-E-035-008 (J.H.H.).

H.-Y. Lin is with the Department of Mechanical Engineering, De Lin Institute of Technology, Tucheng, Taiwan 23646, Republic of China.

J.-H. Huang is with the Department of Mechanical Engineering, Feng Chia University, Taichung, Taiwan 40745, Republic of China.

C.-C. Ma is with the Department of Mechanical Engineering, National Taiwan University, Taipei, Taiwan 10617, Republic of China (e-mail: ccma@ntu.edu.tw).

applications. However, the incorporation of a piezoelectric layer into laminated composites by means of embedding will result in anisotropy and complication of the analysis. The references cited above usually are presented by numerical computation. Very few works in the experimental measurement on the vibration characteristics of the piezolaminated composites have been found, especially in the form of the full-field amplitude measurement. This provides a strong motivation for the present study. In an effort to exploit the performance of the piezolaminated composite structures with an embedded piezoceramic layer, it is necessary to visibly examine the vibration characteristics of the piezolaminated plates from an experimental point of view. For this purpose, the optical interferometer that uses laser as the light source is used to accurately measure the vibration characteristics of the angle-ply laminated composite plates with an embedded piezoceramic layer. Two noncontact and real-time optical methods, the full-field electronic speckle pattern interferometry (ESPI) technique and the pointwise LDV technique, are used in this study.

Because ESPI excels in the stable, noncontact, real-time, and full-field measurement, it has become a powerful tool in the real-time observation of object vibrations and micro deformations. The resulting correlation patterns in ESPI represent contour of constant vibration amplitude or surface displacement. Furthermore, the image data are digitized by a video camera and processed by a digital image processing system for the ESPI method, which eliminates the need of photographic recording and film development process for conventional technique. This allows ESPI to extend its applications to many practical engineering fields. ESPI is a well established technique for vibration analysis. The most convenient and common setup used for vibration measurement by ESPI is the time-averaging method [6] that produces a video image of vibrating object superimposed with correlation fringes that are modulated by the zero order Bessel function of the first kind. In 1971, Butters and Leendertz [7] first applied ESPI to study the vibration modes of circular disc. Although the time-averaging method is powerful for vibration analysis, the limitations of this method are poor image quality, decreased visibility with vibration amplitude, and the lack of the knowledge on vibration phase. Hence, numerous research of further development on the ESPI method have been addressed to overcome these limitations and to extend its use in practical applications. Løkberg and Hogmoen [8] extended the amplitude measurement range by sinusoidal phase modulation of the reference wave in time-averaging ESPI; the information of the vibration phase also was provided. Nakadate [9] used four phase-shifted speckle interferograms to extract numerical data of vibration amplitude. Joenathan and Khorana [10] considered the effect of averaging over a number of video frames and concluded that the contrast of fringes can be optimized with a limited number of superpositions. Anderson *et al.* [11] used a stroboscopic illumination from a frequency modulated (FM) and power modulated (AM) diode laser for vibration analysis. Doval *et al.* [12] developed a technique that used the synchronous stroboscopic illumination combined with simultaneous inter-pulse and inter-frame phase modulation of reference wave in the ESPI system for contrast enhancement and phase control of fringes. Wong *et al.* [13] improved the fringe contrast and sensitivity by subtracting two Bessel fringe patterns at two different force levels. Wang *et al.* [14] proposed the amplitude-fluctuation ESPI (AF-ESPI) technique based on video-signal-subtraction, but the reference image was taken from a vibrating state instead of a free state. The fringe patterns produced by the AF-ESPI method have enhanced visibility and reduced noise. Ma and his coworkers [15]–[17] further developed the AF-ESPI based on the work in [14] and impedance analyzer for three-dimensional vibration analysis of piezoelectric materials.

LDV is based on the principle of the detection of the Doppler shift of coherent laser light that is scattered from a small area of a tested surface. This method has been used to meet various metrology needs for many years. LDV, characterized by an extremely wide signal bandwidth ranging from direct current (DC) to 20 MHz with an ultra-high resolution better than nanometers, appears excellent for the study of piezoelectric materials. However, in obtaining the full-field displacements, the LDV system is much more time-consuming than the ESPI system.

In this study, AF-ESPI and LDV optical systems are used to experimentally investigate the vibration characteristics of the piezolaminated plates with an embedded piezoceramic layer for completely free boundary condition. These piezolaminated plates are excited by applying a time-harmonic voltage to the embedded piezoceramic layer. The resonant frequencies and correspondent mode shapes for piezolaminated plates with five different angle-plies are determined. In addition, in light of the experimental results presented in this work, theoretical predictions based on the finite element method (FEM) using commercial software package ABAQUS (*ABAQUS User's Manual*, ver. 5.8., Pawtucket, RI: Hibbit, Karlsson, and Sorensen, Inc., 1998) also are made. Three different numerical formulations are used to study the vibration characteristics of piezolaminated plates and the influence of the piezoelectric effect on the resonant frequencies is discussed. Excellent agreements of the numerical results in resonant frequencies and mode shapes with experimental data reveal that the presented experimental methodologies are capable of measuring vibration response of piezolaminated plates.

II. Theory of AF-ESPI and LDV Optical Systems for Out-of-Plane Vibration Measurements

ESPI uses the charge-coupled device (CCD) to detect the image plane irradiance distribution of speckle pattern correlation interferogram. The video signal is processed by the digital image processing system, and the resultant correlation fringes are displayed on the monitor. The time-averaging method is the most familiar technique of ESPI used for vibration analysis. The image of a sinusoidally

vibrating object can be described by the irradiance distribution, $I(x,y)$, at the detector array in the CCD camera. The result is expressed as:

$$I = \frac{1}{\tau}\int_0^\tau \left\{ I_O + I_R + 2\sqrt{I_O I_R}\cos \left[\phi + \frac{2\pi}{\lambda}A(1+\cos\theta)\cos\omega t\right]\right\} dt, \quad (1)$$

where I_O and I_R are the irradiance of object and reference fields, respectively, λ is the wavelength of laser, A is the vibration amplitude, ϕ is the random phase difference, θ is the angle between the object light and the observation direction, τ is the CCD refresh time, ω is the angular frequency. Assume that the vibration period is much shorter than the CCD refresh time (i.e., $\tau \gg \frac{2\pi}{\omega}$) and let

$$\Gamma = \frac{2\pi}{\lambda}(1+\cos\theta). \quad (2)$$

And assume $\tau \gg \frac{2m\pi}{\omega}$; m is an integer, then (1) can be reduced to a simplified form as [18]:

$$I_1 = I_O + I_R + 2\sqrt{I_O I_R}(\cos\phi)J_0(\Gamma A), \quad (3)$$

where J_0 is a zero-order Bessel function of the first kind. A very poor quality of fringe pattern is provided by (3) because of the existence of a DC term $(I_O + I_R)$. To remove the DC term in (3), the AF-ESPI method uses an image subtraction procedure that the reference and sequential frame images are taken at the vibrating state. If we assume that the vibration amplitude of the second image has changed from A to $A + \Delta A$ due to the electronic noise or the instability of the apparatus, then the light intensity of the second image can be represented as:

$$I_2 = \frac{1}{\tau}\int_0^\tau \left\{ I_O + I_R + 2\sqrt{I_O I_R}\cos \left[\phi + \Gamma(A+\Delta A)\cos\omega t\right]\right\} dt. \quad (4)$$

Expanding (4) by using the Taylor series expansion, keeping the first two terms and neglecting the higher order terms, we get:

$$I_2 = I_O + I_R + 2\sqrt{I_O I_R}(\cos\phi)\left[1 - \frac{1}{4}\Gamma^2(\Delta A)^2\right]J_0(\Gamma A). \quad (5)$$

When these two images (i.e., I_1 and I_2) are subtracted and rectified by the image processing system, the resulting light intensity can be expressed as:

$$I = |I_2 - I_1| = \frac{\sqrt{I_R I_O}}{2}\left|(\cos\phi)\Gamma^2(\Delta A)^2 J_0(\Gamma A)\right|. \quad (6)$$

Compare the result shown in (6) with that in (3), a good quality of fringe pattern that represents the equal-amplitude displacement contour will be obtained by using the AF-ESPI method. As indicated in (6), the modulation function for the AF-ESPI method is $|J_0(\Gamma A)|$. Hence,

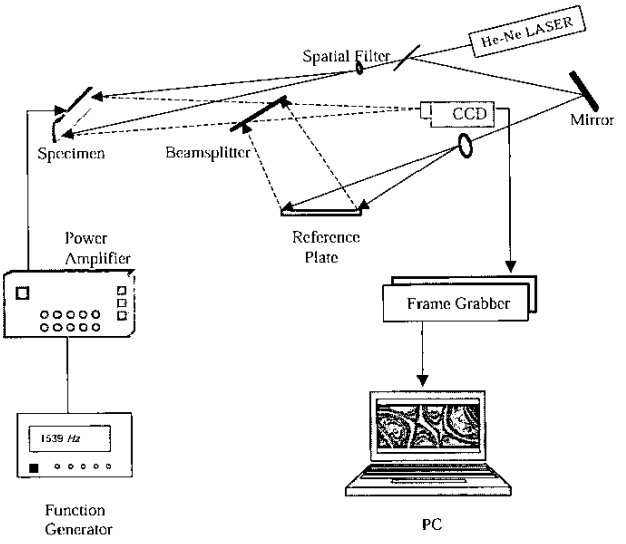

Fig. 1. Diagram of AF-ESPI for out-of-plane measurement.

the nodal lines obtained by the AF-ESPI method are the brightest fringes. The characteristics of the AF-ESPI method can be used as a qualitative observation or quantitative analysis for the fringe patterns. Ma and Huang [16] provided a detailed discussion of the AF-ESPI method for measurement of both out-of-plane and in-plane vibrations. The optical setup for out-of-plane vibration measurement by AF-ESPI is shown in Fig. 1. The complete vibration characteristics of piezolaminated plates, including resonant frequencies and mode shapes, will be discussed in detail by using the AF-ESPI method.

A self-arranged time-averaging ESPI system is used to perform the experimental measurements. As shown in Fig. 1, a He-Ne Laser (25-LHP-928-249, Melles Griot, Carlsbad, CA) with maximum power of 35 mW and wavelength $\lambda = 632.8$ nm is used as the coherent light source. The emitting laser beam is split into two parts by a variable beamsplitter. Acting as an object beam, one beam is directed toward the tested piezolaminated plate then reflects to the CCD camera. The second one, serving as a reference beam, is illuminated on the surface of a reference plate and reflects into the CCD camera via the beamsplitter. Then the object and reference beams are combined into the CCD sensor array through a zoom lens (Nikon Micro-Nikkor 55mm, Nikon, Melville, NY). A CCD camera (Pulnix TM-7CN, Pulnix America, Inc., Sunnyvale, CA) and a frame grabber (Dipix P360F, Dipix Technologies Inc., Ottawa, Ontario, Canada) with a digital signal processor on board are used to record and process the images obtained from interferogram of the object and reference beams. The CCD camera converts the intensity distribution of the interference pattern of the object into a corresponding video signal at 30 frames per second, which was in consequence processed electronically and finally converted into an image on the video monitor. The interpretation of the fringe image is similar to the reading of a displacement contour. To achieve a sinusoidal out-

put, a function generator (HP-33120A, Hewlett Packard, Palo Alto, CA) connected to a power amplifier (NF Electronic Instruments 4005 type, NF Corporation, Kohoku-ku, Yokohama, Japan) is used as an input source, which generates a periodical exciting force to the specimen.

Detailed experimental procedures of the AF-ESPI technique are performed as follows. Once the specimen is vibrating, the interferogram recorded by the CCD camera is stored in an image buffer as a reference image, then the next frame is grabbed and is subtracted by the image processing system. If the vibrating frequency is not at the resonant frequency, only randomly distributed speckles are displayed and no fringe patterns will be shown. In case the vibrating frequency falls in the neighborhood of the resonant frequency, distinct stationary fringe patterns will be observed in the monitor. Then, the function generator is gradually turned with caution to increase the number of fringes until the fringe patterns become clear yet without positional shifts of nodal lines as the resonant frequency is approached. From the aforementioned experimental procedures, the resonant frequencies and the corresponding full-field mode shapes can be determined at the same time by using the AF-ESPI optical system.

The second optical technique used for measuring the dynamic response of piezolaminated plates is a LDV measurement system incorporated with the advanced vibrometer/interferometer device (AVID, Ahead Optoelectronics Inc., Chung-Ho, Taipei, Taiwan). A description of AVID's components and their working principles can be found in great detail in [19]. Instead of using an acoustic optical modulator, the AVID system utilizes circular polarization interference configuration, which can significantly reduce the size of the vibrometer and avoid the radio frequency electromagnetic interference effects created by the high frequency signal required to drive the acoustic optical modulator. With the circular polarization interference technique and digital signal processing with built-in phase decoding algorithms, the system can be applied to measure dynamic displacement and vibration responses of almost any object. The optical system for measuring dynamic displacements in the experiment is based on the principle of the Michelson interferometer and the Doppler effect. A dynamic signal analyzer (DSA) is integrated into the LDV system to become the LDV-DSA system. The DSA unit is composed of the analysis software and a plug-in waveform generator board that can provide the swept-sine excitation signal to the piezolaminated specimen, and the outgoing laser light is directed to a specific point of the upper surface of the specimen. In the analysis software, the swept-sine excitation signal is taken as input, and the response measured by LDV is converted into the voltage signal and is taken as output. After the fast Fourier transform (FFT) processing of the input and output with the DSA software, the ratio of output/input (gain) and the relationship of phase between the input and output signals are obtained. A chart of the data showing the frequency response curve can be obtained. The peak values appearing in the frequency response curve are the resonant frequencies. As a result, we easily can identify the resonant frequencies of piezolaminated plates from the frequency response curve.

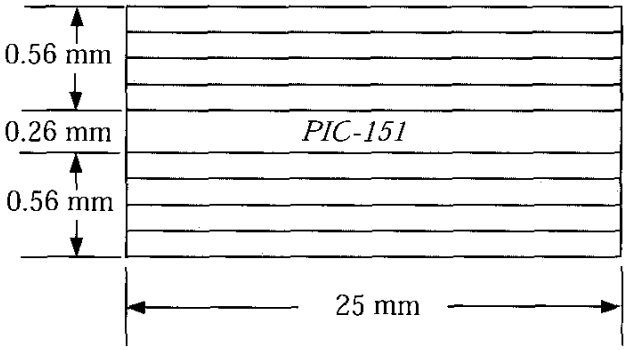

Fig. 2. Diagram for the side-view of the piezolaminated plate.

TABLE I
MATERIAL CONSTANTS OF PIC-151.

Quality	PIC-151
C_{11}^E (N/m^2)	10.76×10^{10}
C_{12}^E	6.313×10^{10}
C_{13}^E	6.386×10^{10}
C_{33}^E	10.04×10^{10}
C_{44}^E	1.962×10^{10}
C_{66}^E	2.224×10^{10}
e_{31} (N/Vm)	-9.52
e_{33}	15.14
e_{15}	11.97
$\rho(Kg/m^3)$	7800
$\varepsilon_{11}^s/\varepsilon_0$	1111
$\varepsilon_{33}^s/\varepsilon_0$	925
ε_0	8.85×10^{-12}

III. EXPERIMENTAL AND NUMERICAL RESULTS

A. Sample Preparation and FEM Method

In this section, the vibration characteristics of angle-ply composite plates with an embedded piezoceramic layer are investigated. These piezolaminated plates with the dimensions of $70 \times 25 \times 1.38$ mm has the stacking sequence $[\theta/-\theta/\theta/-\theta/PIC151/-\theta/\theta/-\theta/\theta]$. Five different stacking angles (i.e., $\theta = 0°$, $30°$, $45°$, $60°$, $90°$) are chosen to make the specimens. Fig. 2 shows its schematic illustration of the specimen; a thin piezoelectric plate made of $Pb(Zr,Ti)O_3$ ceramics with the model number PIC-151 (Physik Instrumente, Lederhose, Germany) is embedded in the middle of the angle-ply, fiberglass-reinforced plastic materials. The material properties of this thin piezoceramic plate are listed in Table I. The two opposite faces of this piezoceramic plate are completely coated with silver electrodes, and the piezolaminated plate is excited by the application of a time-harmonic voltage across electrodes on the two surfaces of the embedded piezoceramic plate.

When the frequency of excitation is near the resonant frequencies of the piezolaminated plate, this specimen is in resonance. The fiberglass used is a continuous filament "E" type (manufactured by the Forthtrack Co., Ltd, Taichung, Taiwan, model number FT-150G). It consists of fiberglass precoated with the thermosetting resin; the composition of epoxy resin and fiberglass is 37% and 63%, respectively. Fabrication of these laminated composite structures involves simply laying-up the prepreg at the required orientation on a forming mold, stacking layers of prepreg in the required stacking sequence, then curing the assembly under elevated temperature and pressure of 130°C and 50 psi for 2 hours. Table II lists the material properties of the fiberglass-reinforced lamina measured by the material-testing system (MTS) and strain gauges, where E_{11} and E_{22} are Young's moduli in the longitudinal and transverse directions, respectively; ν_{12} is the Poisson's ratio; G_{12} is the in-plane shear modulus. To increase the intensity of light reflection of the specimens and the contrast of fringe patterns, the surfaces of the plates are coated with white paint, which is mixed with fine seaweed powder.

In numerical simulation, three formulations based on different models are used to evaluate the vibration characteristics of piezolaminated plates by commercial FEM software ABAQUS. For the FEM I analysis, the plane shell element (S9R5) with nine layers is used to model the vibration behaviors of piezolaminated plates; a local coordinate system for definition of the material properties in each layer is used. FEM II also uses the plane shell element (S9R5), but the piezolaminated plate is treated as an integral part and is partitioned into three sections along the thickness direction. The element S9R5 is a nine-node thin shell element that has five degrees of freedom at the node and imposes the Kirchhoff constraint numerically. To simplify this problem, the top and the bottom parts ($[\theta/-\theta/\theta/-\theta]$ and $[-\theta/\theta/-\theta/\theta]$) are treated as a single homogeneous layer with effective material constants by an averaging process that is commonly used for composite materials [20]. The averaging process in FEM II is performed as follows: Compute the stiffness coefficients for the lamina from Table II. Use tensor transformation for each lamina to obtain transformed lamina stiffness matrix for different fiber orientation. Construct the laminate bending stiffness. Compute the effective engineering constants. The bending stiffness for $[\theta/-\theta/\theta/-\theta]$ laminate is obtained from the material properties of lamina, and the results are shown in Table III. The diagram of the piezolaminated composite plate for this formulation is shown in Fig. 3. The piezoelectric coupling effect is active only in piezoelectric elements, but this piezoelectric effect for the piezoceramic layer is not formulated in FEM I and FEM II. In the ABAQUS package, these elements are available only in the solid (continuum) elements and truss elements. In order to investigate the influence of piezoelectric coupling effect on the vibration behavior of the piezolaminated plates, FEM III uses the solid element (C3D20R) and the three-dimensional piezoelectric element (C3D20RE) to model the behavior of laminated composite layers and the embedded piezoceramic layer, respectively. The elements C3D20R and C3D20RE are 20-node quadratic brick, reduced integration, three-dimensional continuum stress/displacement, and piezoelectric element, respectively. A local coordinate system for definition of material properties is used for the nine-layered structure. It is obvious that the FEM III is more time consuming for the calculation.

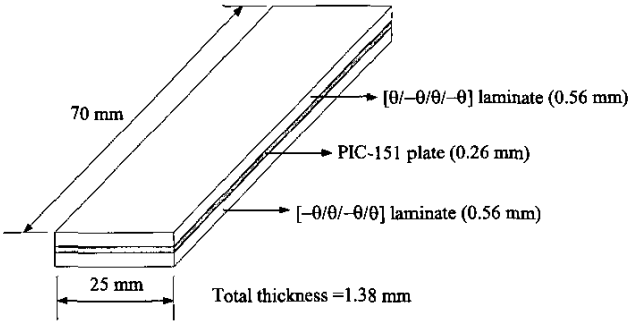

Fig. 3. Geometrical configuration of the piezolaminated plate formulated in FEM II.

B. Comparisons of Experimental and Numerical Results

The resonant frequencies of the first 13 modes for piezolaminated plates with five different fiber orientation measured by AF-ESPI and predicted by FEM are listed in Tables IV, V, VI, VII, and VIII. The mode shapes and the excitation voltage used in the experimental measurement for each mode are also indicated in these tables. Only a slight difference in the resonant frequencies obtained by FEM I and FEM II is found. This indicates that the use of effective engineering constants for simulation of inhomogeneous multilayer structure as a homogeneous single layer is feasible and useful. By comparing the results obtained by FEM I and FEM III, it is interesting to note that most of the results predicted by the solid model (FEM III) are smaller than those of shell model (FEM I and FEM II). In general, the introduction of the piezoelectric effect will increase the rigidity of the specimen. This phenomenon can be verified by the results listed in Table IX. Those results shown in the column of excluding piezoelectric effects are computed numerically by using the solid stress element (C3D20R) for both the composite layers and the embedded piezoelectric layer. In other words, the piezoelectric effect is insignificant. It is found that the piezoelectric effect only leads to a slighter increase in the rigidity of piezolaminated plates. Hence, in comparison with the results by FEM I and FEM II, the decrease of resonant frequencies in FEM III is not caused by the piezoelectric effect. This is mainly because the transverse shear stresses in solid elements do not vanish at the free surface and are discontinuous along the interfaces. By comparing the results of AF-ESPI and FEM, it is found that the experimental results are consistently greater than the numerical results for the lower frequencies. This might be due to the fact

TABLE II
MATERIAL CONSTANTS OF FIBERGLASS REINFORCED LAMINA (UNIDIRECTIONAL).

Material properties	E_{11} Gpa	E_{22} Gpa	ν_{12}	G_{12} Gpa	ρ
Magnitude	36.11	8.8	0.32	3.48	$1820\left(kg/m^3\right)$

TABLE III
EFFECTIVE ENGINEERING CONSTANTS OF VARIOUS ANGLE-PLY LAMINATES.

Engineering constants Fiber orientation	E_x (Gpa)	E_y (Gpa)	G_{xy} (Gpa)	ν_{xy}
$[0° - 0°/0° - 0°]$	36.11	8.8	3.48	0.32
$[30° - 30°/30° - 30°]$	19.56	8.64	8.42	0.707
$[45° - 45°/45° - 45°]$	10.973	10.973	10.071	0.577
$[60° - 60°/60° - 60°]$	8.64	19.56	8.42	0.312
$[90° - 90°/90° - 90°]$	8.8	36.11	3.48	0.078

TABLE IV
RESULTS OF RESONANT FREQUENCIES OBTAINED FROM AF-ESPI AND FEM FOR THE $[0/-0/0/-0/PIC151/-0/0/-0/0]$ PIEZOLAMINATED PLATE.[1]

	AF-ESPI (excitation voltage)	FEM I (error %)	FEM II (error %)	FEM III (error %)
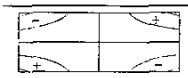	961 Hz (6.04 V)	897.4 (−6.61)	897.4 (−6.61)	898.7 (−6.48)
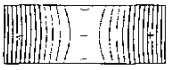	1073 (6.04 V)	1017.2 (−5.20)	1017.2 (−5.20)	1015.9 (−5.32)
	2158 (15.09 V)	2101.6 (−2.61)	2101.6 (−2.61)	2094.9 (−2.92)
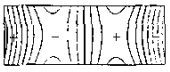	2837 (10.06 V)	2804.9 (1.13)	2804.9 (1.13)	2786.9 (−1.77)
	—	3939.8 (—)	3939.8 (—)	3903.6 (—)
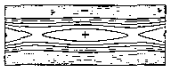	4361 (16.10)	4062.6 (−6.84)	4062.6 (−6.84)	4055.3 (−7.01)
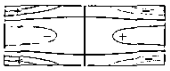	4729 (16.10 V)	4462.7 (−5.63)	4462.7 (−5.63)	4443.8 (−6.03)
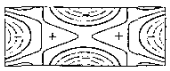	5525 (17.61 V)	5430.8 (1.70)	5430.8 (1.70)	5362.4 (−2.94)
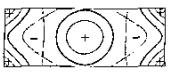	5950 (21.13 V)	5725.9 (−3.77)	5725.9 (−3.77)	5660.7 (−4.86)
	—	6444.4 (—)	6444.4 (—)	—
	6529 (25.15 V)	6608.7 (1.22)	6608.7 (1.22)	6497.3 (−0.49)
	7461 (55.33 V)	7501.8 (0.55)	7501.8 (0.55)	7376.5 (−1.13)
	9018 (30.18 V)	9172.4 (1.71)	9172.4 (1.71)	8951.5 (−0.74)

[1]Error: compared with AF-ESPI method.

TABLE V
RESULTS OF RESONANT FREQUENCIES OBTAINED FROM AF-ESPI AND FEM FOR THE [30/ − 30/30/ − 30/$PIC$151/ − 30/30/ − 30/30] PIEZOLAMINATED PLATE.[1]

	AF-ESPI (excitation voltage)	FEM I (error %)	FEM II (error %)	FEM III (error %)
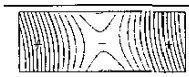	848 Hz (5.03 V)	751.9 (−11.33)	763.88 (−9.92)	763.0 (−10.02)
	1473 (15.09 V)	1354.9 (−8.02)	1356.6 (−7.90)	1333.6 (−9.46)
	2249 (15.09 V)	2126.5 (−5.45)	2167.1 (3.64)	2150.4 (−4.38)
	3064 (15.09 V)	2879.2 (−6.03)	2878.0 (−6.07)	2820.7 (−7.94)
	4314 (50.3 V)	3998.9 (−7.30)	4043.3 (−6.27)	4006.1 (−7.14)
	4660 (35.21 V)	4543.4 (−2.50)	4731.7 (1.54)	4611.4 (−1.04)
	5012 (25.15 V)	4887.3 (−2.49)	—	—
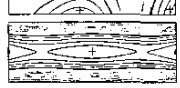	5415 (12.58 V)	—	4734.7 (−12.6)	4695.1 (−13.30)
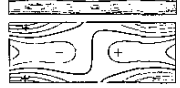	5730 (7.54 V)	5126.6 (−10.53)	5132.8 (−10.4)	5047.4 (−11.91)
	6960 (6.54 V)	6806.7 (2.20)	7068.6 (1.56)	6847.1 (−1.62)
	—	7219.4 (—)	7235.5 (—)	7019.8 (—)
	7531 (12.58 V)	7528.8 (0.03)	7404.1 (2.35)	7251.5 (−3.70)
	—	9717.6 (—)	9972.6 (—)	9593.0 (—)

[1]Error: compared with AF-ESPI method.

that the soft sponge support has a significant influence on the resonant frequencies, which is neglected in the FEM simulation. Analytically, boundary condition can be specified as completely free or any constrained situations. The completely free boundary means that the specimen is, in fact, floating in space with no attachment or connection in ground and exhibits rigid body behavior at zero frequency. In testing practice, however, it is almost not realizable and generally not possible to fully achieve this condition. Hence, the specimen must be supported in some manner to model the completely free boundary. In this study, to experimentally model the completely free boundary, the piezoelectric plate is placed on the surface of a very soft sponge with the dimensions $80 \times 60 \times 23$ mm and is stuck to the two lateral sides by a narrow adhesive tape on the surface of sponge.

Figs. 4–6 show the first 13 modes obtained by ESPI and FEM for piezolaminated plates. The theoretical prediction of the mode shapes presented in Figs. 4–6 is based on the results for FEM I. The excellent quality of the interferometric fringe pattern obtained from the AF-ESPI method is demonstrated. For the finite element results as shown in Figs. 4–6, the dashed lines and the — sign indicate the concave displacements; the solid lines and the + sign denote convex displacements. The transition from solid lines to dashed lines corresponds to a zero displacement line or a nodal line that is represented as a bold, black line. The zero-order fringes, which are the brightest fringes on the experimental results, represent the nodal lines of the piezolaminated plate at resonant frequencies. The rest of the fringes are contours of constant displacements. The mode shapes obtained from the experimental results can be verified by the nodal lines and fringe patterns with the numerical finite element calculations. Excellent agreement of the experimental measurement and numerical calculation are observed for all the vibration modes. The related amplitude A_i, $i = 1, 2, 3, 4 \ldots, n$ for the ith fringe in the experimental results can be quantitatively calculated by the

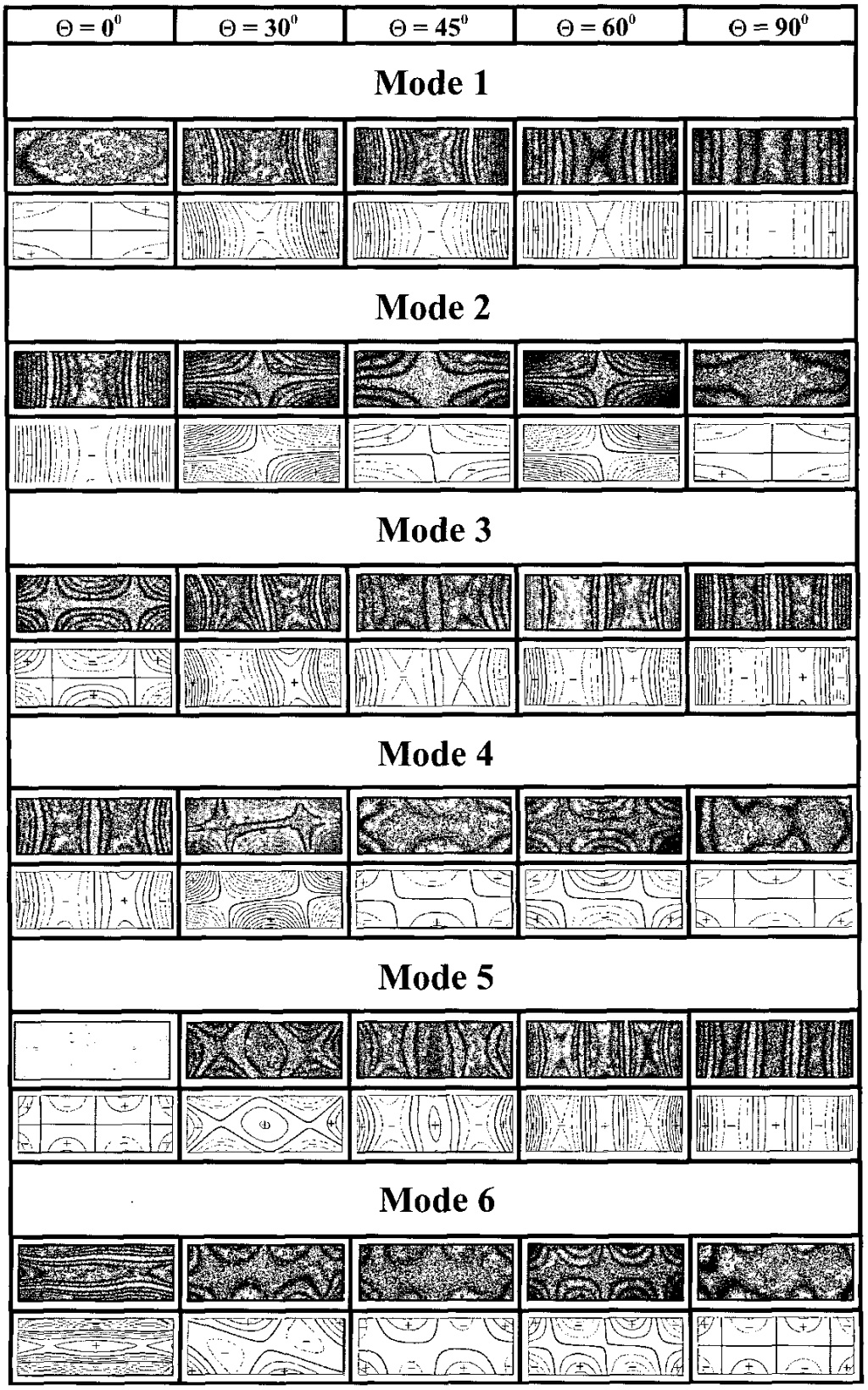

Fig. 4. Mode shapes of the laminated composite plate with an embedded piezoceramic layer obtained by AF-ESPI and FEM. Modes 1 to 6.

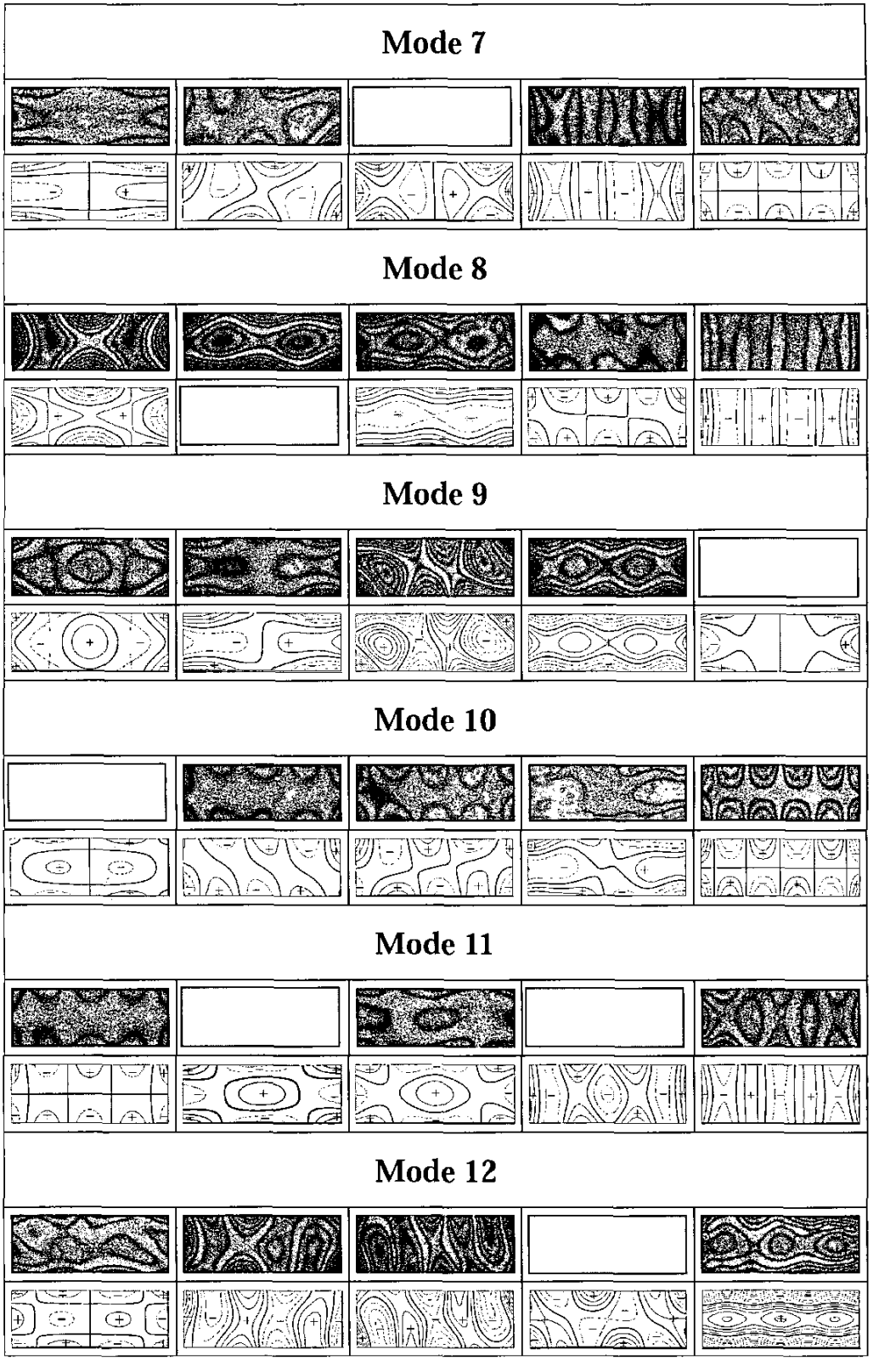

Fig. 5. Mode shapes of the laminated composite plate with an embedded piezoceramic layer obtained by AF-ESPI and FEM. Modes 7 to 12.

TABLE VI
RESULTS OF RESONANT FREQUENCIES OBTAINED FROM AF-ESPI AND FEM FOR THE $[45/-45/45/-45/PIC151/-45/45/-45/45]$ PIEZOLAMINATED PLATE.[1]

	AF-ESPI (excitation voltage)	FEM I (error %)	FEM II (error %)	FEM III (error %)
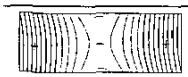	648 Hz (3.02 V)	579.6 (−10.56)	582.4 (−10.12)	582.1 (−10.17)
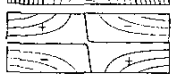	1471 (25.15 V)	1453.7 (1.18)	1471.9 (0.06)	1441.2 (−2.03)
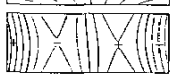	1746 (30.18 V)	1673.7 (−4.14)	1685.4 (−3.47)	1672.4 (−4.22)
	2983 (30.18 V)	3016.1 (1.11)	3053.6 (2.37)	2981.4 (−0.05)
	3510 (30.18 V)	3331.7 (−5.08)	3357.1 (−4.36)	3315.1 (−5.55)
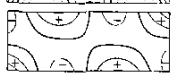	4687 (27.67 V)	4774.7 (1.87)	4852.8 (3.54)	4713.8 (0.57)
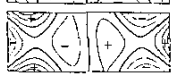	—	5345.1 (—)	5374.7 (—)	5266.5 (—)
	5496 (25.15 V)	5363.2 (−1.98)	5337.3 (−2.89)	5293.4 (−3.69)
	6388 (17.61 V)	6365.2 (0.36)	6484.4 (1.51)	6365.2 (−0.36)
	6736 (20.12 V)	6991.1 (3.79)	6969.6 (3.47)	6726 (−0.15)
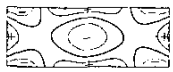	7698 (25.15 V)	7897.8 (2.60)	7955.8 (3.34)	7686.4 (−0.15)
	8439 (25.15 V)	8839.4 (4.74)	9066.1 (7.43)	8843.1 (4.79)
	9083 (25.15 V)	9560.6 (5.26)	9486.0 (4.43)	9089.1 (0.07)

[1]Error: compared with AF-ESPI method.

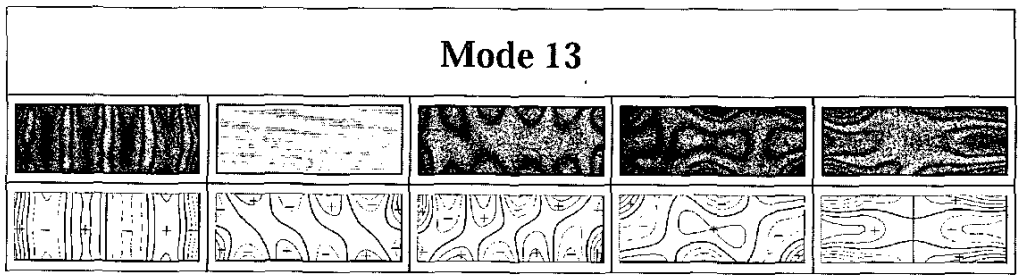

Fig. 6. Mode shapes of the laminated composite plate with an embedded piezoceramic layer obtained by AF-ESPI and FEM. Mode 13.

TABLE VII
RESULTS OF RESONANT FREQUENCIES OBTAINED FROM AF-ESPI AND FEM FOR THE [60/ − 60/60/ − 60/$PIC$151/ − 60/60/ − 60/60] PIEZOLAMINATED PLATE.[1]

	AF-ESPI (excitation voltage)	FEM I (error %)	FEM II (error %)	FEM III (error %)
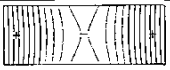	596 Hz (11.07 V)	512.8 (−14.05)	513.1 (−13.91)	514.0 (−13.76)
	1281 (7.55 V)	1323.6 (3.32)	1345.0 (5.00)	1321.3 (3.14)
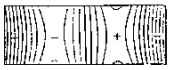	1517 (6.04 V)	1445.5 (−4.71)	1447.2 (−4.60)	1444.1 (−4.81)
	2673 (7.55 V)	2739.6 (2.49)	2781.2 (4.05)	2725.9 (1.98)
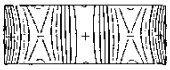	3048 (10.06 V)	2875.2 (−5.67)	2880.0 (−5.51)	2862.9 (−6.07)
	4143 (15.59 V)	4333.3 (4.59)	4394.5 (6.07)	4290.8 (3.57)
	4877 (32.70 V)	4780.1 (−1.99)	4789.6 (−1.79)	4740.4 (−2.80)
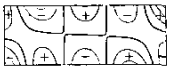	5924 (32.70 V)	6167.7 (4.11)	6263.4 (5.73)	6086.9 (2.75)
	6524 (22.64 V)	6439.6 (−1.29)	6437.6 (−1.32)	6363.3 (−2.46)
	7087 (25.15 V)	7127.4 (0.57)	7112.0 (0.35)	6989.0 (−1.38)
	—	7369.1 (—)	7395.2 (—)	7284.0 (—)
	—	8329.4 (—)	8458.2 (—)	8178.2 (—)
	8479 (25.15 V)	8792.7 (3.70)	8768.7 (3.42)	8531.0 (0.6)

[1]Error: compared with AF-ESPI method.

roots of $J_0(\Gamma A) = 0$ as indicated in (6). We use $\theta = 10°$ for the experimental setup and $\lambda = 632.8$ nm; the related vibration amplitudes for the first six dark fringes are A_i, $i = 1 \sim 6$, $= 0.12$, 0.28, 0.44, 0.6, 0.76, and 0.92 μm. Note that the vibration displacements obtained in this study are in the order of submicrometer.

It is found that the sequence of the first and the second, the third and the fourth mode shape of the piezolaminated plate for $\theta = 0°$ interchanges as compared with other fiber orientations. The eighth and the ninth mode shapes for $\theta = 0°$ fiber orientation cannot be observed in other fiber orientations. It can be concluded that the vibrating behavior of the piezolaminated plate for $\theta = 0°$ is different from other piezolaminated plates. It is worth noting that the sequence of all 13 modes for five different fiber orientations calculated from FEM I is almost the same as that obtained by the experimental observation. However, eight vibration modes (i.e., the fifth and the tenth modes for $\theta = 0°$, the eleventh and the thirteenth modes for $\theta = 30°$, the seventh mode for $\theta = 45°$, the eleventh and the twelfth modes for $\theta = 60°$, the ninth mode for $\theta = 90°$) cannot be observed by AF-ESPI. This discrepancy can be attributed to the fact that these modes are not easily excited by the embedded piezoceramic plate so that the amplitude is beyond the sensitivity of the AF-ESPI optical system. It is indicated in Tables IV, V, and VIII that two modes (i.e., the tenth mode for $\theta = 0°$ and the ninth mode for $\theta = 90°$) which cannot be observed by AF-ESPI are not predicted by FEM III either; the eighth mode for $\theta = 30°$ is not predicted by FEM I but is observed by both AF-ESPI and FEM III.

In order to have a better understanding of the reason that causes the discrepancies of these modes, a second experimental optical method, the LDV that is a point-wise displacement measurement technique, is used to investigate the vibration characteristics of piezolaminated plates. The LDV system has an extremely wide signal bandwidth and an ultra-high resolution that is in the order of nanome-

TABLE VIII
RESULTS OF RESONANT FREQUENCIES OBTAINED FROM AF-ESPI AND FEM FOR THE [90/ − 90/90/ − 90/$PIC$151/ − 90/90/ − 90/90] PIEZOLAMINATED PLATE.[1]

	AF-ESPI (excitation voltage)	FEM I (error %)	FEM II (error %)	FEM III (error %)
	615 Hz (6.04 V)	514.1 (−16.4)	514.1 (−16.4)	515.8 (−16.10)
	926 (10.06 V)	874.9 (−3.46)	874.9 (−3.46)	876.5 (−5.34)
	1539 (10.06 V)	1418.8 (−3.90)	1418.8 (−3.90)	1421.0 (−7.67)
	1932 (17.61 V)	1862.3 (−1.35)	1906 (−1.35)	1860.8 (−3.68)
	3096 (17.61 V)	2784.2 (−6.27)	2784.2 (−6.27)	2782.0 (−10.14)
	3234 (30.18 V)	3064.7 (−2.75)	3064.7 (−2.75)	3052.1 (−5.62)
	4733 (10.06 V)	4571.2 (−0.11)	4571.2 (−0.11)	4537.2 (−4.14)
	5037 (25.15 V)	4605.1 (−4.73)	4605.1 (−4.73)	4587.7 (−8.92)
	—	6446 (—)	6446 (—)	—
	6765 (20.12 V)	6450.6 (−1.61)	6450.6 (−1.61)	6381.8 (−5.54)
	7231 (7.55 V)	6870.3 (−1.06)	6870.3 (−1.06)	6820.1 (−5.68)
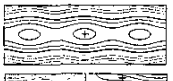	7841 (26.16 V)	8073.6 (3.04)	8073.6 (3.04)	7955.8 (1.46)
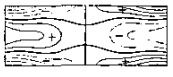	8106 (25.15 V)	8236.6 (1.78)	8236.5 (1.78)	8109.7 (0.05)

[1]Error: compared with AF-ESPI method.

ters. A built-in DSA composed of software and a plug-in function generator board is included in the LDV system that can provide the swept-sine excitation signal. The swept-sine excitation signal is taken as input, the response measured by LDV is taken as output. After the FFT processing of the input and output with the DSA software, the ratio of output/input (gain) is obtained. A chart that shows the frequency response curve can be obtained. The peak values appeared in the frequency response curve are the resonant frequencies. The beginning and ending sweeping frequencies in the LDV-DSA system are set from 10 and 7210 Hz. The sampling point at every frequency span is 360, and the frequency response curves of these piezolaminated plates are shown in Figs. 7–11. The resonant frequencies emerge clearly at the peak values in these figures. The peak values also are indicated in Table X for comparison with those obtained by the AF-ESPI for the first 10 resonant frequencies. We can see that the mea-

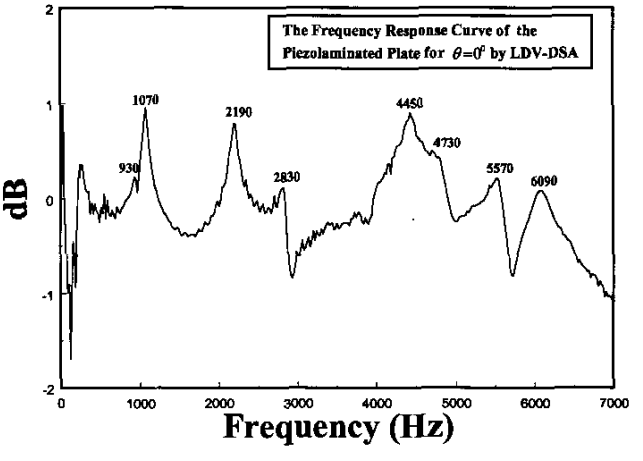

Fig. 7. Frequency response curve obtained by LDV-DSA for the [0/ − 0/0/ − 0/$PIC$151/ − 0/0/ − 0/0] piezolaminated plate.

TABLE IX
THE INFLUENCE OF PIEZOELECTRIC EFFECT ON THE RESONANT FREQUENCIES FOR PIEZOLAMINATED PLATES BY SOLID MODEL FORMULATION.

$\theta = 0°$			$\theta = 30°$		
Mode	Include piezoelectric effect (Hz)	Exclude piezoelectric effect (Hz)	Mode	Include piezoelectric effect (Hz)	Exclude piezoelectric effect (Hz)
1	898.7	898.5	1	763	762.2
2	1015.9	1014.3	2	1333.6	1333.3
3	2094.9	2093	3	2150.4	2146.9
4	2786.9	2782	4	2820.7	2819
5	3903.6	3897.5	5	4006.1	3839
6	4055.3	4008.1	6	4611.4	4605.1
7	4443.8	4398.3	7	4695.1	4660.2
8	5362.4	5346.2	8	5047.4	5015.8
9	5660.7	5619.1	9	6847.1	6837
10	6497.3	6484.1	10	7019.8	6987
$\theta = 45°$			$\theta = 60°$		
Mode	Include piezoelectric effect (Hz)	Exclude piezoelectric effect (Hz)	Mode	Include piezoelectric effect (Hz)	Exclude piezoelectric effect (Hz)
1	582.1	580.8	1	514	510.7
2	1441.2	1441.0	2	1321.3	1321
3	1672.4	1666.8	3	1444.1	1434
4	2981.4	2979.7	4	2725.9	2723.9
5	3315.1	3302.4	5	2862.9	2841.6
6	4713.8	4708.6	6	4290.8	4284.2
7	5266.5	5248.4	7	4740.4	4704.6
8	5293.4	5258.8	8	6086.9	6072
9	6365.2	6325.3	9	6363.3	6335.8
10	6726	6714.8	10	6989	6960.7

$\theta = 90°$		
Mode	Include piezoelectric effect (Hz)	Exclude piezoelectric effect (Hz)
1	515.8	510.4
2	876.5	876.2
3	1421	1405.8
4	1860.8	1858.1
5	2782	2751.7
6	3052.1	3042.8
7	4537.2	4515.6
8	4587.7	4536.8
9	6381.8	6341
10	6820.1	6745.2

sured results by these two optical methods agree well. Table X indicates that the resonant frequencies which cannot be observed from the AF-ESPI are not measured by the LDV-DSA system, either. Hence, the resonant frequencies determined by the AF-ESPI method are correct and are verified by the LDV-DSA system.

Fig. 12 illustrates the variation of the resonant frequencies for the first five modes with different angle of fiber orientation. The maximum rigidity mostly occurs at $\theta = 30°$ and 45° for the first five vibration modes. The measured results of resonant frequencies obtained by experimental AF-ESPI and LDV-DSA methods agree well with numerical predictions. Therefore, the experimental techniques with the characteristics of high efficiency and full-field configuration, such as the AF-ESPI method proposed in this study, can be used to provide a better understanding of the complete vibration behavior for piezolaminated plates.

IV. CONCLUSIONS

The vibration characteristics of piezolaminated plates are important in many engineering applications. However, there are only a few experimental results available in the literature. This study has examined experimentally the resonant frequencies and mode shapes of vibrating piezolaminated plates by using the self-arranged AF-ESPI optical setup and LDV-DSA system. It has shown that the two optical methods have the advantages of noncontact, real-time, and high-resolution measurement for investigat-

TABLE X
FIRST 10 RESONANT FREQUENCIES OBTAINED BY AF-ESPI AND LDV-DSA.[1]

	$\theta = 0°$	$\theta = 30°$	$\theta = 45°$	$\theta = 60°$	$\theta = 90°$
Method Mode	AF-ESPI (LDV-DSA) [error %]	AF-ESPI (LDV-DSA) [error %]	AF-ESPI (LDV-DSA) [error %]	AF-ESPI (LDV-DSA) [error %]	AF-ESPI (LDV-DSA) [error %]
1	961 (930) [−3.23]	848 (870) [2.59]	648 (630) [−2.78]	596 (590) [−1.01]	615 (610) [−0.81]
2	1073 (1070) [−0.28]	1473 (1430) [−2.92]	1471 (1490) [1.29]	1281 (1270) [−0.86]	926 (930) [0.43]
3	2158 (2190) [1.48]	2249 (2250) [0.04]	1746 (1790) [2.52]	1517 (1510) [−0.46]	1539 (1550) [0.71]
4	2837 (2830) [−0.25]	3064 (3030) [−1.11]	2983 (3030) [1.58]	2673 (2670) [−0.11]	1932 (1970) [1.97]
5	—	4314 (4310) [−0.09]	3510 (3550) [1.14]	3048 (3090) [1.38]	3096 (3070) [−0.84]
6	4361 (4450) [2.04]	4660 (4750) [1.93]	4687 (4790) [2.20]	4143 (4190) [1.13]	3234 (3190) [−1.36]
7	4729 (4730) [0.02]	5012 (4970) [−0.84]	—	4877 (5010) [2.73]	4733 (4810) [1.63]
8	5525 (5570) [0.81]	5415 (5370) [−0.83]	5496 (5530) [0.62]	5924 (5970) [0.78]	5037 (5110) [1.45]
9	5950 (6090) [2.35]	5730 (5610) [−2.09]	6388 (6470) [1.28]	6524 (6670) [2.24]	—
10	—	6960 (7090) [1.87]	6736 (6930) [2.88]	7087 (7130) [0.61]	6765 (6790) [0.37]

[1]Error: compared with AF-ESPI method.
Unit: Hz

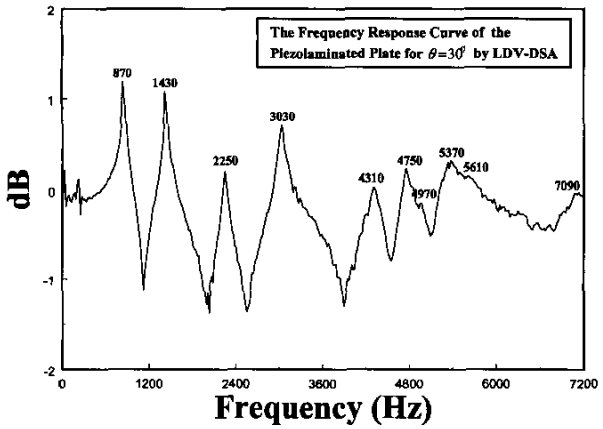

Fig. 8. Frequency response curve obtained by LDV-DSA for the $[30/-30/30/-30/PIC151/-30/30/-30/30]$ piezolaminated plate.

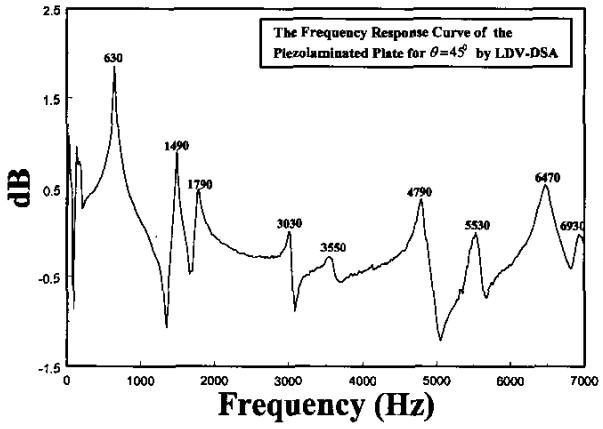

Fig. 9. Frequency response curve obtained by LDV-DSA for the $[45/-45/45/-45/PIC151/-45/45/-45/45]$ piezolaminated plate.

ing the vibration problem of piezolaminated plates. High-quality interferometric fringes for mode shapes are presented by a video recording system for the AF-ESPI. The resonant frequencies are determined rapidly by the LDV-DSA system. According to our results, the resonant frequencies and full-field mode shapes up to 13 modes measured by AF-ESPI and LDV correlate well with the FEM results. Some mode shapes that are difficult to be excited by the embedded piezoceramic layer are identified from the experimental observation. Discrepancies of the prediction

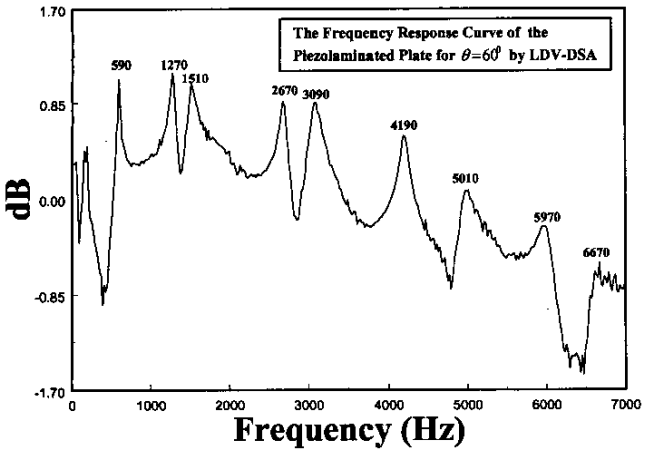

Fig. 10. Frequency response curve obtained by LDV-DSA for the $[60/-60/60/-60/PIC151/-60/60/-60/60]$ piezolaminated plate.

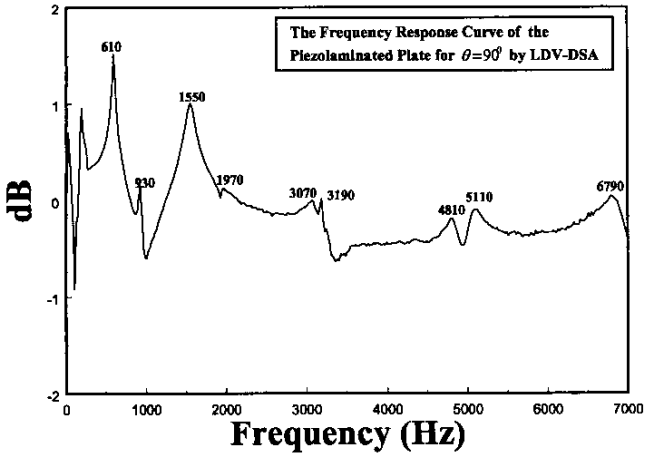

Fig. 11. Frequency response curve obtained by LDV-DSA for the $[90/-90/90/-90/PIC151/-90/90/-90/90]$ piezolaminated plate.

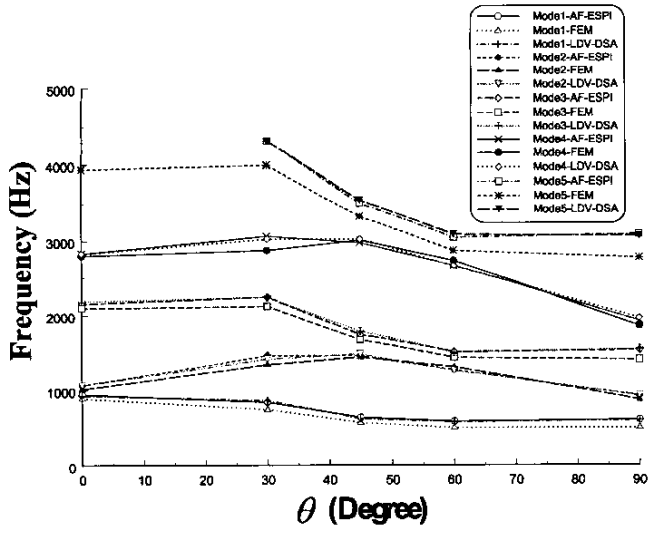

Fig. 12. Comparison of the first five resonant frequencies of piezolaminated plates obtained by AF-ESPI, LDV-DSA, and FEM I.

of resonant frequencies by different FEM formulations are observed and are discussed. Many unexplored issues for the vibration characteristics of piezolaminated plates are addressed with discussions in detail. The results obtained in this study also demonstrate that the optical techniques proposed herein are applicable in the vibration analysis for piezolaminated plates.

REFERENCES

[1] S. K. Ha, C. Keilers, and F. K. Chang, "Finite element analysis of composite structures containing distributed piezoceramic sensors and actuators," *AIAA J.*, vol. 30, no. 3, pp. 772–780, 1992.

[2] H. Abramovich and A. Livshits, "Dynamic behavior of cross-ply laminated beams with piezoelectric layers," *Composite Struct.*, vol. 25, no. 1-4, pp. 371–379, 1993.

[3] R. C. Batra and X. Q. Liang, "Vibration of a rectangular laminated elastic plate with embedded piezoelectric sensors and actuators," *Comput. Struct.*, vol. 63, no. 2, pp. 203–216, 1997.

[4] P. Bhattacharya, H. Suhail, and P. K. Sinha, "Finite element free vibration analysis of smart laminated composite beams and plates," *J. Intell. Mater. Syst. Struct.*, vol. 9, no. 1, pp. 20–28, 1998.

[5] M. A. R. Loja, J. I. Barbosa, C. M. Mota Soares, and C. A. Mota Soares, "Analysis of piezolaminated plates by the spline finite strip method," *Composite Struct.*, vol. 79, no. 26-28, pp. 2321–2333, 2001.

[6] R. Jones and C. Wykes, *Holographic and Speckle Interferometry*. Cambridge, England: Cambridge Univ. Press, 1989.

[7] J. N. Butters and J. A. Leendertz, "Speckle patterns and holographic techniques in engineering metrology," *Opt. Laser Technol.*, vol. 3, no. 1, pp. 26–30, 1971.

[8] O. J. Løkberg and K. Hogmoen, "Use of modulated reference wave in electronic speckle pattern interferometry," *J. Phys. E: Sci. Instrum.*, vol. 9, no. 10, pp. 847–851, 1976.

[9] S. Nakadate, "Vibration measurement using phase-shifting speckle pattern interferometry," *Appl. Opt.*, vol. 25, no. 22, pp. 4162–4167, 1986.

[10] C. Joenathan and B. M. Khorana, "Contrast of vibration fringes in time-averaged electronic speckle pattern interferometry: Effect of speckle averaging," *Appl. Opt.*, vol. 31, no. 11, pp. 1863–1870, 1992.

[11] D. J. Anderson, J. D. Valera, and J. D. C. Jones, "Electronic speckle pattern interferometry using diode laser stroboscopic illumination," *Eng. Opt.*, vol. 6, no. 4, pp. 475–480, 1993.

[12] A. F. Doval, J. L. Fermández, M. Pérez-Amor, J. D. R. Valera, and J. D. C. Jones, "Contrast enhanced and phase controlled stroboscopic additive fiber optic tv-holography for whole field out-of-plane vibration analysis," *Opt. Lasers Eng.*, vol. 25, no. 4-5, pp. 323–342, 1996.

[13] W. O. Wong, K. T. Chan, and T. P. Leung, "Contrast and sensitivity of the vibration fringes in time-averaged electronic speckle-pattern interferometry: Effect of variations of force level," *Opt. Laser Technol.*, vol. 29, no. 4, pp. 179–185, 1997.

[14] W. C. Wang, C. H. Hwang, and S. Y. Lin, "Vibration measurement by the time-averaging electronic speckle pattern interferometry method," *Appl. Opt.*, vol. 35, no. 22, pp. 4502–4509, 1996.

[15] C. H. Huang and C. C. Ma, "Vibration characteristics for piezoelectric cylinders using amplitude-fluctuation electronic speckle pattern interferometry," *AIAA J.*, vol. 36, no. 12, pp. 2262–2268, 1998.

[16] C. C. Ma and C. H. Huang, "The investigation of three-dimensional vibration for piezoelectric rectangular parallelepipeds using the AF-ESPI method," *IEEE Trans. Ultrason., Ferroelect., Freq. Contr.*, vol. 48, no. 1, pp. 142–153, 2001.

[17] C. H. Huang and C. C. Ma, "Experimental measurement of mode shapes and frequencies for vibration of plates by optical interferometry method," *ASME J. Vib. Acoust.*, vol. 123, no. 2, pp. 276–280, 2001.

[18] C. M. Vest, *Holographic Interferometry*. New York: Wiley, 1976.

[19] C. K. Lee and G. Y. Wu, "High performance doppler interferometer for advanced optical storage system," *Jpn. J. Appl. Phys.*, vol. 38, no. 3B, pp. 1730–1741, 1999.
[20] M. W. Hyer, *Stress Analysis of Fiber-Reinforced Composite Materials*. Singapore: McGraw-Hill, 1998.

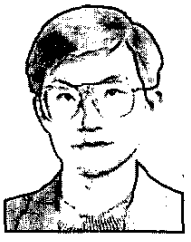

Hsien-Yang Lin received the B.S. degree in civil engineering from the Feng Chia University, Taichung, Taiwan, in 1984, and the M.S. and Ph.D. degrees in mechanical engineering from the National Taiwan University, Taipei, Taiwan, Republic of China, in 1989 and 2001, respectively. Since 1990, he has been with the De Lin Institute of Technology, Taipei, Taiwan, Republic of China, where he is currently an associate professor of mechanical engineering.

His research interests include the photomechanics, and vibration analysis of piezoceramic materials.

Jin H. Huang received the B.S. degree in mechanical engineering from the Feng Chia University, Taichung, Taiwan, Republic of China, the M.S. degree in mechanical engineering from the University of New Mexico, Albuquerque, NM, and the Ph.D. degree in mechanical engineering from Northwestern University, Evanston, IL, in 1985, 1989, and 1992, respectively. Since 1993 he has been with the Feng Chia University, where he is currently a professor of mechanical engineering.

His research interests include the application of piezoelectric/piezomagnetic composites, magnetostriction of ferromagnetic composites, and effective material properties of composites.

Chien-Ching Ma received the B.S. degree in agriculture engineering from the National Taiwan University, Taipei, Taiwan, in 1978 and the M.S. and Ph.D. degrees in mechanical engineering from Brown University, Providence, RI in 1982 and 1984, respectively. From 1984 to 1985, he worked as a postdoc in the Engineering Division, Brown University. In 1985, he joined the faculty of the Department of Mechanical Engineering, National Taiwan University, Taiwan, Republic of China, as an associate professor. He was promoted to full professor in 1989.

His research interests are in the fields of wave propagation in solids, fracture mechanics, solid mechanics, and vibration analysis.